Modelling contrast sensitivity of discs

Maliha Ashraf; University of Liverpool, UK
Rafał Mantiuk; University of Cambridge, UK
Alexandre Chapiro; Meta, USA

Abstract

Spatial and temporal contrast sensitivities are typically measured using different stimuli. Gabor patterns are used to measure spatial contrast sensitivity and flickering discs are used for temporal contrast sensitivity. The data from both types of studies is difficult to compare as there is no well-established relationship between the sensitivity to disc and Gabor patterns. The goal of this work is to propose a model that can predict the contrast sensitivity of a disc using the more commonly available data and models for Gabors. To that end, we measured the contrast sensitivity for discs of different sizes, shown at different luminance levels, and for both achromatic and chromatic (isoluminant) contrast. We used this data to compare 7 different models, each of which tested a different hypothesis on the detection and integration mechanisms for discs. The results indicate that multiple detectors contribute to the perception of disc stimuli, and each can be modelled either using an energy model, or the peak spatial frequency of the contrast sensitivity function.

Introduction

Contrast sensitivity explains the visibility of low-contrast patterns and is an important indicator of performance of the visual system. There have been multiple attempts to model an all-encompassing function of contrast sensitivity [1, 2, 3, 4, 5], which could predict the visibility thresholds for stimuli of a given spatial and temporal frequency, luminance, size, orientation, eccentricity and modulation along different directions in a colour space. To model all these dimensions, it is necessary to combine contrast sensitivity measurements from multiple sources, often obtained using different procedures and varying stimuli. The two dominant types of stimuli are Gabor patterns, typically used for the measurement of spatial contrast sensitivity, and discs, which are used to measure temporal contrast sensitivity. Combining spatial and temporal sensitivity data is problematic as there is no established model that can explain the detection of discs from Gabor data or vice-versa. Our goal is to propose such a model.

This work is also a step towards building a contrast sensitivity function for edges. Edges are important image feature, which are arguably more relevant for practical applications than Gabor patterns or sinusoidal gratings. However, it is unclear how the contrast sensitivity of an edge can be predicted from contrast sensitivity functions fitted to data for Gabor patches. To address this problem, we measured detection threshold for discs of three different sizes, shown at different luminance levels (from 0.002 to 200 $\mathrm{cd/m^2}$), with achromatic contrast and two chromatic contrast directions (red-grey and violet-grey). Next, we fit six models that predict disc sensitivity using a contrast sensitivity function for spatio-chromatic Gabor patterns [4]. The results indicate that multiple detectors contribute to the detection of a disc and each detector can be modelled either using an energy model, or the peak spatial frequency of the contrast sensitivity function.

Related work

Numerous studies over the years, have measured contrast sensitivity across a very large parameter space. It varies along spatial frequency [6, 7, 8], temporal frequency [9, 10, 11], luminance level [12, 9, 13, 14], colour direction [15, 16, 14], stimulus size [9, 17, 18, 13], retinal eccentricity [19, 20], stimulus shape and grating profile [7, 21, 22, 18], and orientation [23, 24, 25]. Many studies have presented contrast sensitivity data along different combinations of the aforementioned parameters but the measurements can be difficult to compare due to slight differences in methodology and the data covering a different part of the parameter space. Some of these differences in measurements can be compensated by a constant offset in sensitivity [5]. Differences in pupil diameter can be compensated using standard models [26]. However, when the stimuli differ considerably, a simple offset or multiplier cannot account for the differences.

Most achromatic and chromatic temporal contrast sensitivity studies have used a fixed-aperture flickering stimulus to measure the temporal contrast sensitivity [27, 28, 29, 11, 30, 31]. In addition to contrast sensitivity, flicker sensitivity measurements are a widely used measure to characterise temporal vision. Most older studies investigating this use a simple backlight temporal modulation with a fixed aperture resulting in a disk shaped stimulus [32, 33, 34]. To be able to compare these fixed-aperture stimuli with the more physiologically-motivated stimuli (e.g., Gabor patches), we need a model that can integrate the sensitivities from fundamental components to predict the thresholds of more complex stimuli.

Since the visual system is composed of channels that are tuned to different spatial frequencies and orientations [7, 35], the combined sensitivities of these individual channels can be used to predict sensitivities of more complex stimuli. In their seminal work, Campbell and Robson (1968) proposed the spatially-selective multi-channel model of the human vision system by comparing contrast thresholds from sine and square wave gratings. They proposed a simple relationship between contrast sensitivities of high-frequency square and sine waves [7]. Here, we test this simple model on disk stimuli. Watson and Ahumada (2005) proposed a relatively simple energy summation model to predict the contrast sensitivity of different spatial stimuli [22]. Their model performs very well for a variety of different achromatic spatially-varying stimuli. However, the model has not been demonstrated to work across luminance levels, stimulus sizes and for chromatic contrast modulation. This work validates the energy model for such a variety of conditions.

Experiment: disc CSF

Displays Our study was carried out using three different displays, two in Liverpool and one in Cambridge. The complete set of measurements was collected on an Eizo ColorEdge CS2740 27" 4K LCD monitor in Cambridge. This monitor could be calibrated with very high accuracy and was driven with a 10 bit signal. Further 2 bits were simulated by spatio-temporal dithering. To reproduce luminance levels below 1 cd/m^2, the observers wore a modified pair of goggles with neutral density (ND) filters (Kodak Wratten Gelatin 2.0D). A few select conditions were measured by a larger number of participants on either a custom-HDR display (described in [14]) or an LG G2 55" OLED display in Liverpool. Goggles with a 2.1 ND filter were used to measure 0.2 cd/m^2 conditions on the OLED display. All displays were colour-calibrated prior to measurement. CIE2006 cone fundamentals [36] were used to generate colour stimuli. We used three different displays to ensure that the measurement are consistent across different devices. A chin rest was used to control the viewing distance (1.07 m in Cambridge).

Stimuli The stimuli were circular disks of different sizes, luminance level and colour directions. Some examples of those are shown in Figure 1. The stimuli varied along the following parameters:

- Luminances: 0.02, 0.2, 2, 20 and 200 cd/m^2
- Sizes: 0.0833, 0.5 and 2 deg diameter disks
- Colour directions: luminance (C1), pinkish red (C2) and violet (C3) directions were the three cardinal colour directions in the DKL colour space [37]. C1 is an achromatic stimulus with contrast changing only along the luminance direction. C2 and C3 contrasts are isoluminant (with respect to the background) modulated along the positive directions of the DKL colour space. We did not attempt to find individual isoluminant plane via heterochromatic flicker photometry as we were interested in models that could generalise beyond individual measurements.

The background for all stimuli was D65 grey with the corresponding mean luminance level and had the size of $31.2\times17.9^\circ$ (Cambridge).

Experimental procedure Initial estimates of contrast sensitivities were recorded via a method of adjustment where the observers were asked to adjust the contrast of each of the stimuli until they could just detect it. This initial estimate was the prior for the the next adaptive 4AFC stage. In the 4AFC stage, the observers were shown a 2x2 grid, with only one quadrant containing the stimulus. The presentation time was not limited. The observers indicated which quadrant contained the stimulus and their response drove the QUEST adaptive sampling method [38] implemented in PsychToolBox-3 [39]. The responses were fitted with a psychometric function and the contrast level with 0.84 probability of correct responses was chosen as the threshold contrast for the specific stimulus.

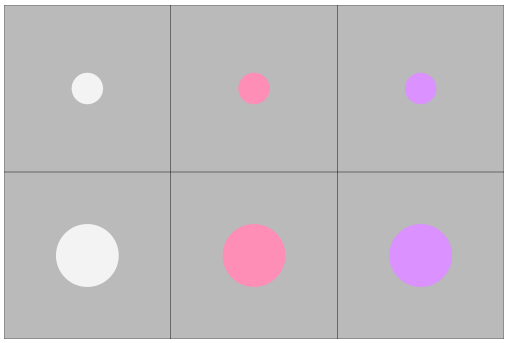

Figure 1. *Example disc stimuli used in the experiment*

A single luminance level was measured at a time. The observers were asked to adapt for 3 minutes to the lowest luminance (0.02 cd/m^2), one minute to 0.2 cd/m^2 and 30 seconds for other luminance levels. The sizes and colour directions were randomised across the QUEST trials.

Participants 3 colour normal observers and one deutan took part in the experiment in Cambridge. The deutan observer completed only the conditions for the achromatic disc. A further 6 observers participated in Liverpool for a reduced number of conditions. The data collected in Liverpool was meant to test reproducibility and estimate variance across the population.

Results The individual measurements are shown as small markers in Figure 4. The means were computed over all the data collected in Cambridge and Liverpool. The inter-observer variability across the devices used in Cambridge and Liverpool was found to be comparable. Table 1 reports the standard deviations in dB for the data.

Table 1. *Mean of inter-observer standard deviation for all stimuli. Standard deviations from two of the devices separately is also reported. Only one observer participated in experiment with the device liverpool-HDR, so the variance is not reported.*

	All devices	Cam-Eizo	Liv-OLED
SD [dB]	2.9687	2.7678	2.7126

A one-way ANOVA was performed to test if there were significant differences in contrast measurements between the three devices. Luminance, spatial frequency, and stimulus size were random effects in the model. No statistically significant difference was found between the measurements from the difference devices ($F(2,283) = 0.1026, p = 0.9025$).

Our data shows that contrast sensitivity increases with luminance and the size of the disc (Figure 4) for all measured colour directions. To test the statistical significance of these effects, we performed a n-way ANOVA with log of luminance and size (along with their two-way interaction) as fixed effects and colour direction, device, and observers as random effects. The combined effect of luminance and size was found to be statistically significant ($F(1,282) = 6.3668), p < 0.05$).

Contrast energy models

First, we will review a family of contrast energy models [22] that attempt to predict the sensitivity to a disk. The contrast energy model assumes that a pattern is detected when the energy of that pattern exceeds a pre-determined threshold. The energy is computed as

$$E = \int_{\rho_x}\int_{\rho_y} \left(I(\rho_x,\rho_y)\,S(\rho_x,\rho_y)\right)^2 d\rho_x\,d\rho_y\,, \tag{1}$$

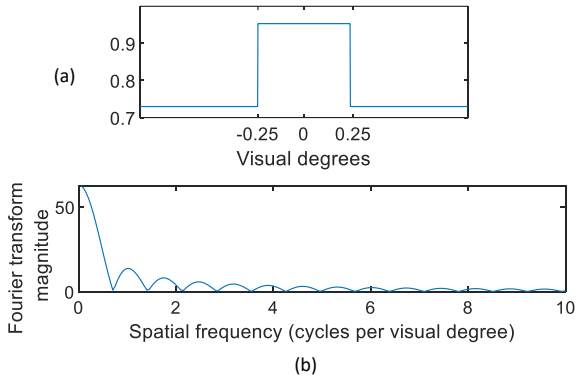

Figure 2. *Decomposition of disk stimuli into sinusoids in Fourier space. (a) 1D representation of disk stimulus in spatial domain; (b) Fourier transform magnitude of the disk stimulus in spatial frequency domain. The transform of rectangular pulse is sinc function.*

where ρ_x and ρ_y are the horizontal and vertical spatial frequencies in cycles per degree (cpd), I is the Fourier transform of a signal (Fourier transform of a luminance map) and S is a contrast sensitivity function.

To model the frequency decomposition of a disc, we can take its cross section, which forms a rectangular function as shown in Figure 2. The analytical Fourier transform of a rectangular function is a sinc function:

$$D(\rho;r) = r\,\mathrm{sinc}(2\,\rho\,r) \tag{2}$$

where r is the radius of the disc in visual degrees and ρ is the spatial frequency in cycles per degree. To avoid integration in both spatial dimensions, as done in Eq. (1), we can integrate the energy in the polar coordinates ($\rho = \sqrt{\rho_x^2+\rho_y^2}, \theta$):

$$\begin{aligned} E(r,L_\mathrm{b},c) &= \int_0^{2\pi}\int_\rho \left(c\,D(\rho;r)\,S(\rho,L_\mathrm{b},a)\right)^2 \rho\,d\rho\,d\theta \\ &= 2\pi c^2 \int_\rho \left(D(\rho;r)\,S(\rho,L_\mathrm{b},a)\right)^2 \rho\,d\rho\,, \end{aligned} \tag{3}$$

where $S()$ is the contrast sensitivity as the function of spatial frequency ρ, luminance of the background L_b and area a. The last term ρ serves as the Jacobian determinant. c is the contrast of the disc expressed as a Weber ratio, $\Delta L/L_\mathrm{b}$. The disc is detected when the energy exceeds the threshold energy, E_thr, therefore the detection threshold can be found as:

$$c_\mathrm{thr} = \sqrt{\frac{E_\mathrm{thr}}{E(r,L_\mathrm{b},1)}} \tag{4}$$

We compute the contrast sensitivity as the inverse of the detection threshold, $s = 1/c_\mathrm{thr}$.

We use the spatio-chromatic CSF from [4] as function $S()$. This model relies on data from 5 separate datasets, measured from 0.0002 cd/m^2 to 10 000 cd/m^2, and is capable of predicting contrast sensitivity for modulation in any direction in the colour space. We query the colour direction corresponding to the achromatic or chromatic contrast of the disc. This CSF does not model the effect of orientation, and therefore the energy summation in Eq. (3) is assumed to be orientation-independent.

Model fitting and practical considerations

The integral from Eq. (3) is approximated by a numerical integration between 0 and 32 cpd. We found that the predictions are stable at 128 samples. To fit each model described below, we minimise the prediction error:

$$20\sqrt{\frac{1}{N}\sum_{i=1}^{N}\left(\log S_\mathrm{predicted}[i] - \log S_\mathrm{measured}[i]\right)^2} \quad [\mathrm{dB}] \tag{5}$$

for N data points. For S_measured, we used the mean of the data measured across the three displays and all observers. For all models, we fit the threshold energy separately for the achromatic and two chromatic colour directions.

One difficulty with the energy model from Eq. (3) is the choice of the area parameter for the contrast sensitivity function. Below we review several models that differ in the way stimuli are integrated over spatial area.

Disc area

If we assume that the detection of a disc is mostly determined by its low-frequency components, the detection should depend on the size of the disc. Therefore, we can set the area parameter of the CSF to be proportional to the area of the disc: $a \propto \pi r^2$. Unfortunately, we cannot optimise for the proportionality constant, as the area parameter is too strongly correlated with E_thr parameters (optimisation results in very large areas). Instead, we assumed that $a = \pi r^2$.

Constant area

We can argue that the area parameter is irrelevant for the contrast energy model as the model itself accounts for spatial pooling by integrating over area. This is because the integration over the frequency domain in Eq. (3) is equivalent to an integration over spatial area (Plancherel theorem).

We tried to fit a constant-area model by optimising for the area parameter of the CSF, but this resulted in an implausible large value (900 deg^2). Therefore, we instead set this parameter to 1.

Sinc local extrema

One major inconvenience of modelling a disc as a sinc function is that it requires a numerical solution to an integral from Eq. (3). We tested a more convenient model, in which the integral is approximated by summing up the CSF-weighted energy only for the local minima and maxima of the sinc function.

Sum of Gabors

Most CSF models, including the one we use in this work, explain the sensitivity to Gabor patches rather than to isolated spatial frequencies. The sensitivity to isolated frequency can only be measured for an infinite-size grating. The Fourier transform of a Gabor patch is a Gaussian function in the frequency domain — it occupies a band of frequencies rather than a single frequency in the Fourier domain. This raises a question, whether we can approximate the sinc function with a sum of Gabors, or a sum Gaussian functions in the frequency domain.

Figure 3a shows that indeed the sinc function can be well approximated as a sum of multiple Gaussian curves. We can express

Table 2. *Base values of Gaussian curves parameters for the central and the next 5 sinc function lobes as depicted in Figure 3a.*

Sinc lobe (n)	0	1	2	3	4	5
ρ_n	0	1.43	2.46	3.47	4.48	5.48
σ_n	0.5	0.37	0.36	0.35	0.35	0.34
h_n	1	-0.22	0.13	-0.09	0.07	-0.06

the sinc function from Equation 2 as a series:

$$D_{\mathrm{g}}(\rho;r) = \sum_{n=0}^{\infty} h_n \exp\left(-\frac{\left(\rho-\frac{\rho_n}{2r}\right)^2}{2\left(\frac{\sigma_n}{2r}\right)^2}\right), \tag{6}$$

The peak (ρ_n), deviation (σ_n) and height (h_n) of the Gaussian functions are fixed and the first few values are listed in Table 2. The total contrast energy for this model can be represented as a numerical integral with respect to the spatial frequencies corresponding to the peaks of the sinc lobes. Equation 3 then becomes:

$$\begin{aligned} E(r,L_{\mathrm{b}},c) &= 2\pi c^2 \sum_{n=0}^{\infty} \frac{f(n-1)+f(n)}{2}\Delta\rho_n, \\ \text{where, } f(n) &= \left(D_{\mathrm{g}}(\rho_n;r)\,S(\rho_n,L_{\mathrm{b}},a_n)\right)^2\rho_n, \\ a_n &= \pi\left(\frac{r}{\pi\sigma_n}\right)^2 = \frac{1}{\pi}\left(\frac{r}{\sigma_n}\right)^2 \end{aligned} \tag{7}$$

a_n is the area of the corresponding patch which is directly proportional to the radius of the disk and inversely proportional to the standard deviation of the Gaussian curve in Fourier domain.

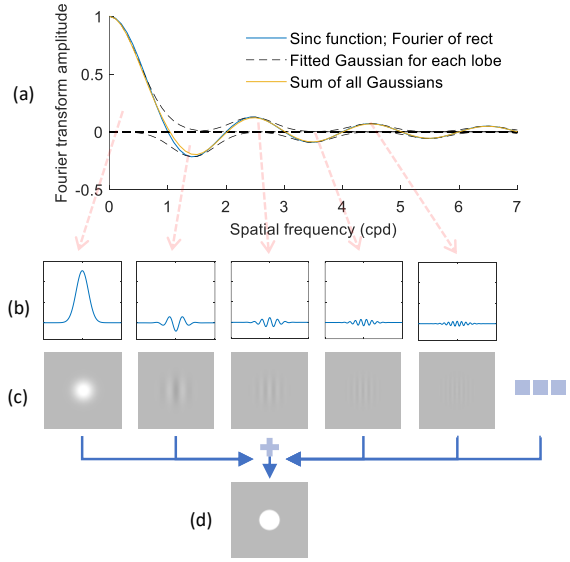

Figure 3. *Decomposition of disk stimuli into Gabor patches in Fourier space. (a) Sinc function as a sum of Gaussian curves; (b) Sinusoids modulated with a Gaussian envelope are the 1D spatial domain representation for each sinc lobe (Gaussian curve). The position of peak in the Fourier space represents the spatial frequency of the sinusoid, the height of the Gaussian is the amplitude of the sinusoid and the standard deviation of the Fourier Gaussian represents the width of the Gaussian envelope in spatial domain; (c) Representative Gabor patches for each lobe of the Fourier transform in (a); (d) 2D achromatic disk stimulus.*

Multiple detector models

Foley at el. demonstrated that the detection of Gabor patches of different sizes, shapes (circular, collinearly and orthogonally elongated) and phases can be explained by detection by one or more mechanisms that are characterised by a receptive field that sums contrast linearly followed by a nonlinear transformation to a response [40]. Here, we extend that idea to model the detection of discs. However, instead of modelling an array of receptive fields, as done in their work, we derive an analytical detection model for a disc.

We assume that when detecting a disc, we detect mainly its edge. Lets assume that a single piece of such an edge is detected by a single hypothetical edge detector. When a disc radius is increased, the edge gets larger and more detectors have a chance to detect it. Such contribution of multiple detectors is typically modelled as probability summation, which corresponds to a generalised sum[1]:

$$s_{\mathrm{all}} = \left(s_1^\beta + s_2^\beta + s_3^\beta + \ldots + s_N^\beta\right)^{1/\beta}, \tag{8}$$

where $s_1, \ldots, s_N$ are the sensitivities of individual detectors. β is the exponent of the psychometric function, typically between 3 and 4. For convenience, we assume that the edge detectors are identical and we perform summation in the continuous domain. Therefore, if all detectors along the circumference of a disc with the radius r contribute, the sensitivity is:

$$s_{\mathrm{all}} = \left(2\pi r s_{\mathrm{ed}}^\beta\right)^{1/\beta} = (2\pi r)^{1/\beta} s_{\mathrm{ed}}, \tag{9}$$

where s_{ed} is the sensitivity of a single edge detector. Below we consider several candidate models for the individual edge detector.

Fundamental frequency

Campbell and Robson demonstrated that the detection of the square wave can be explained by the detection of the fundamental frequency of that square wave [7]. Although we are interested in the detection of discs rather than square waves, we could assume that a single edge detector in a multiple-detector model detects a pattern similar to a square wave. This is because the cross-section of a disk is a rectangular function, and a square wave consists of tiled copies of rectangular functions.

The Fourier series representation of a square wave is composed of a set of sine waves with decreasing amplitude and increasing frequency. For a 50% duty cycle square wave of a specified spatial frequency, the Fourier series representation would be the fundamental component (sine wave) with the same spatial frequency as the square wave and a series of odd harmonics with spatial frequencies in odd multiples (3x, 5x, 7x, ...) of the fundamental. Campbell and Robson showed that for higher spatial frequencies, the sensitivity of a square is $4/\pi$ times the sensitivity of a sine wave with the same fundamental frequency. This relationship remains valid as long as the third harmonic component remains below the detection threshold. Given that, the multiple detector model can be expressed as:

$$S_{\mathrm{disc}}(L_{\mathrm{b}},r) = S_c\,(2\pi r)^{1/\beta}\,\frac{4}{\pi}\,S\left(\frac{1}{4r},L_{\mathrm{b}},a\right), \tag{10}$$

[1] see for example "Luminance intrusion" section in [14]

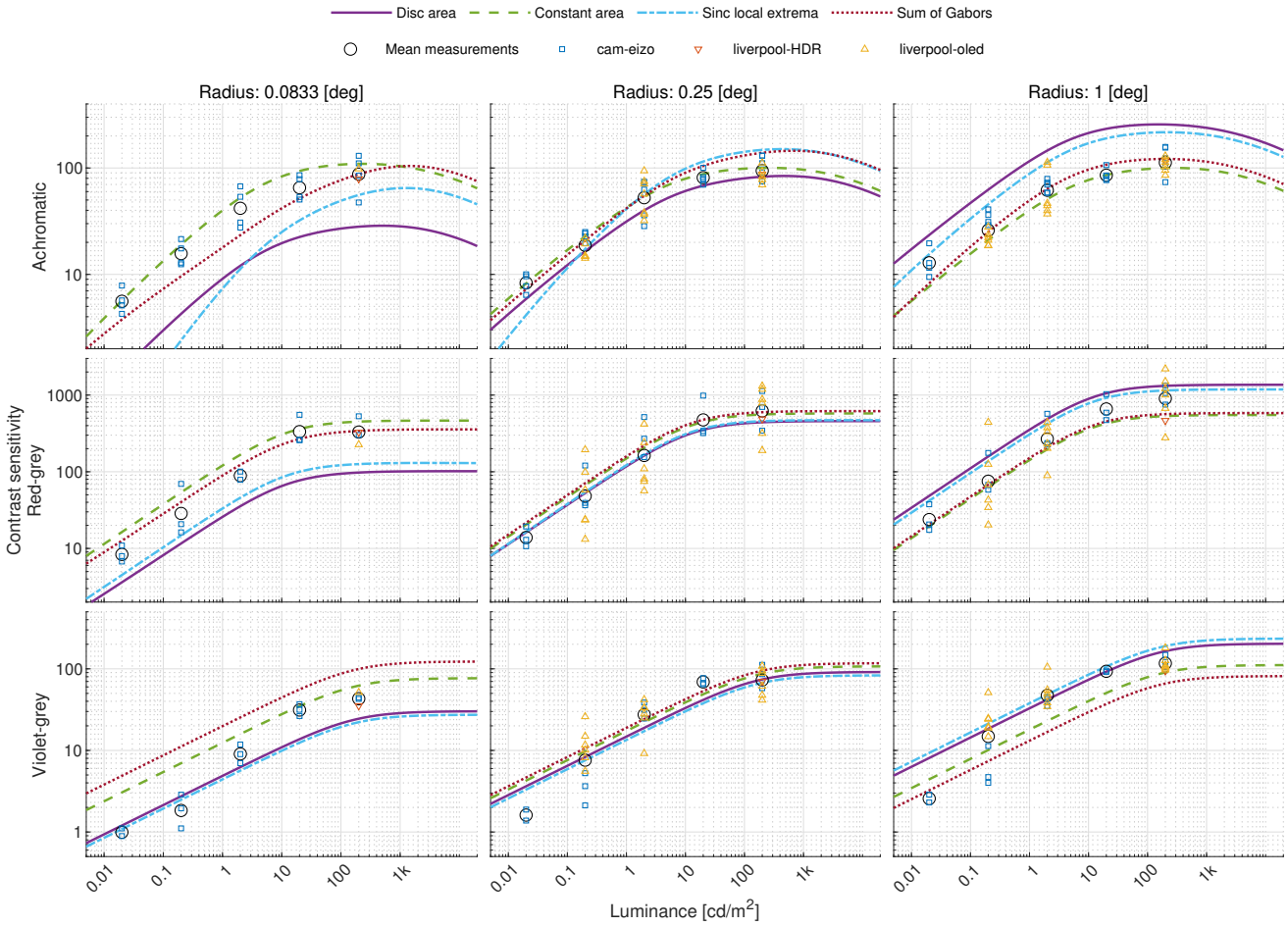

Figure 4. *Measurements of the disc contrast sensitivity and the predictions of the four contrast energy models.*

The spatial frequency, $1/4r$, is selected so that the rectangual function formed by the cross-section of the disc corresponds to a square wave. We tested variations of the model where the area is either a function of the radius of the disc $a = \pi r^2$, set to a constant value $a = 1$ or fitted as a parameter of the model. We also tested the model with different β values. The model provided the best predictions when both the area and the β parameter were optimised in conjunction. However, the optimised value of $\beta = 1.24$ is not realistic for a Weibull psychometric function. So, we fixed $\beta = 3.5$ and fitted the area and the S_c parameters; the fitted values are reported in Table 4.

Peak spatial CSF

Edge contrast sensitivity has been shown to be an indicator of the most sensitive contrast vision channel [41, 42]. In other words, the peak of the contrast sensitivity envelope (across spatial frequencies) is proportional to the edge sensitivity of the visual system. Since a disc forms a circular edge, we can combine the peak-sensitivity assumption with the multiple-detectors model to predict the disc sensitivity as:

$$S_{\text{disc}}(L_\text{b}, r) = S_c \, (2\pi r)^{1/\beta} \max_\rho (S(\rho, L_\text{b}, a)) \,, \tag{11}$$

where S_c is the fitted base sensitivity for a particular colour direction and β is optimised as a parameter of the model, listed in

Table 3. *Parameters and error of fitting each contrast energy model. The threshold energy, E_{thr} is reported for achromatic, red-grey and violet-grey colour directions. The error is reported in the units of dB (see Eq. (5)).*

Model	$E^{\text{ach}}_{\text{thr}}$	$E^{\text{rg}}_{\text{thr}}$	$E^{\text{vg}}_{\text{thr}}$	a	Error
Disc area	0.1639	0.0826	0.0864	n/a	6.78
Constant area	0.4805	0.2533	0.1758	1	4.99
Sinc local extrema	0.1925	0.0917	0.0502	1	6.74
Sum of Gabors	0.3213	0.1495	0.1353	n/a	5.62

Table 4.

Multiple contrast energy detectors

We can combine the multiple detector model with the energy model. Assuming that the inner integral of Eq. (3) represents an individual edge detector, we have:

$$E(r, L_\text{b}, c) = c^2 \, (2\pi r)^{1/\beta} \int_\rho (D(\rho; r) \, S(\rho, L_\text{b}, a_0))^2 \, \rho \, d\rho \,, \tag{12}$$

where a is the nominal (fitted) area, so that $S(\rho, L_\text{b}, a_0)$ models the sensitivity of a single edge detector (s_ed). β was optimised as a parameter of the model.

Results and discussion

The numerical errors and the fitted parameters for our contrast energy models are summarised in Table 3. In terms of nu-

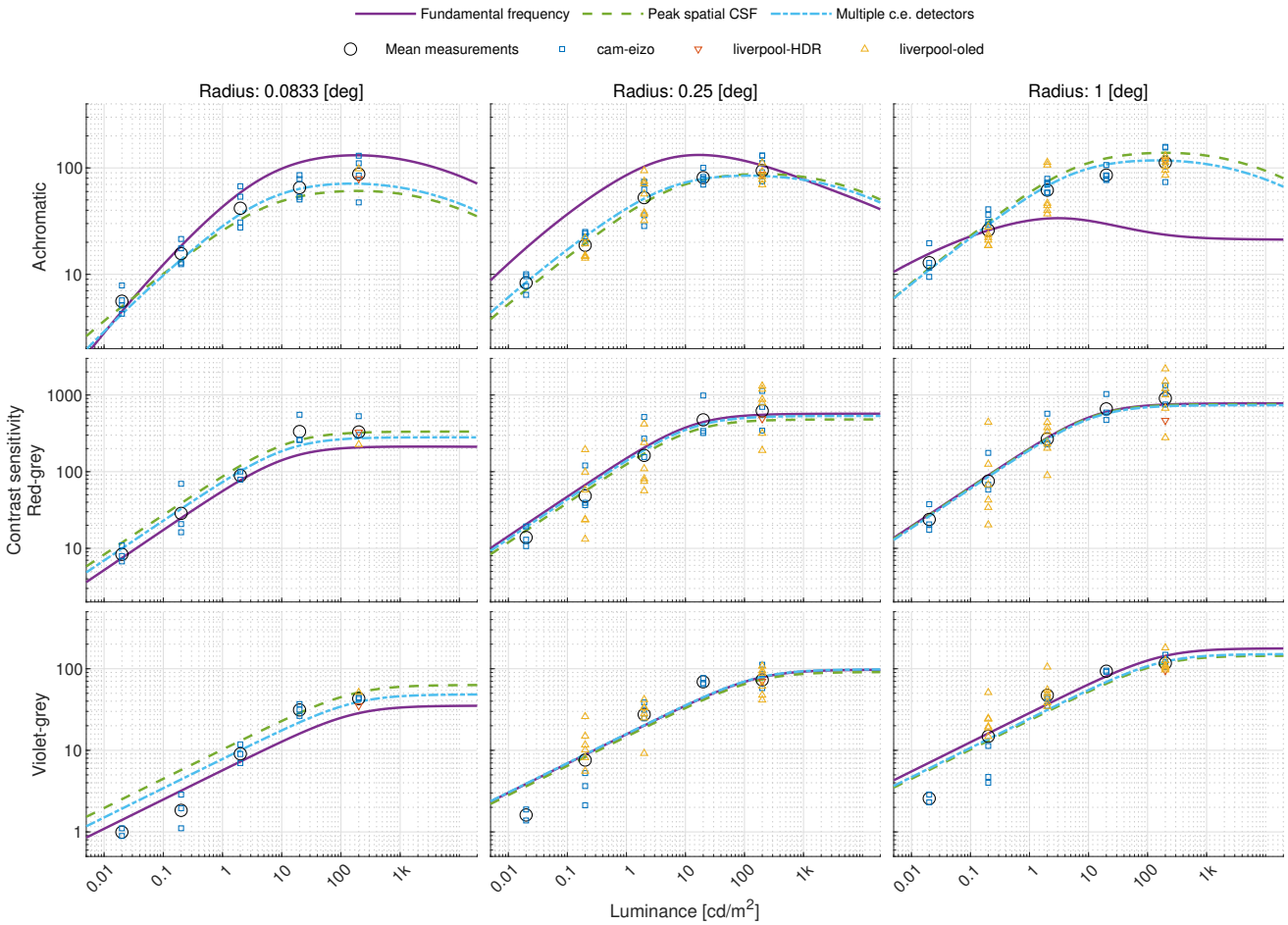

Figure 5. *Measurements of the disc contrast sensitivity and the predictions of the three multiple detectors models.*

Table 4. *Parameters and error of fitting each multiple detectors model. The threshold energy, E_{thr} and base sensitivity, S_c is reported for achromatic, red-grey and violet-grey colour directions. The error is reported in the units of dB (see Eq. (5)).*

Model	S_c^{ach}	S_c^{rg}	S_c^{vg}	a	β	Error
Fundamental frequency	0.6967	0.8040	1.1020	6.94	3.5	6.01
Peak spatial CSF	0.5641	0.9429	1.2404	2.42	3.01	4.54
	$E_{\text{thr}}^{\text{ach}}$	$E_{\text{thr}}^{\text{rg}}$	$E_{\text{thr}}^{\text{vg}}$			
Multiple c.e. detectors	2.1066	0.7460	0.4044	3.63	4.08	4.39

merical error, the *disc area* model is the worst performing, while the *constant area* model has the lowest prediction error among the four contrast energy models. The predictions, shown in Figure 4, demonstrate that the sensitivity to disc type stimuli does not increase with the disc radius as rapidly as predicted by the *disc area* model. Therefore, we can discard the hypothesis that the detection of the disc is mostly mediated by the detection of the low-frequency signal formed by a disc. The *constant area* model predicts the data better than the disc area model. However, this model does not account for the small increase of sensitivity with the radius of the disc. In case of the *sinc local extrema* model, the summation over a discrete set of frequencies poorly predicts the sensitivity to discs. And our last contrast energy model, *sum of gabors* does not predict the data as well as the *constant area* model despite the theoretical premise that a disc can be approximated by a series of Gabors.

Figure 5 and Table 4 show the fitting results for the three proposed multiple detectors models. Numerically, the *fundamental frequency* multiple detectors model, performs worse than the *constant area* and *sum of gabors* models but better than *disc area* and *sinc local extrema* models. Qualitatively, the fitting results of the *fundamental frequency* model show that the shape of the CSF with respect to luminance is distorted as the radius of the disc stimuli increases, as depicted in the top-right panel in Figure 5. The assumption that the contrast sensitivity of a disc could be approximated as a function of square wave contrast sensitivity could be valid for smaller sized disc stimuli only.

Multiple c.e. detectors and *peak spatial CSF* models have the lowest two error values respectively among all our proposed models. Increasing the size of a disc has a small effect on sensitivity that is well modelled assuming probability summation across multiple detectors, shown in Eq. (9). This is the strategy used in both our best-performing models. The fitting errors of both models (4.39 and 4.54 dB) are comparable, as well as the curves shown in Figure 5. The available data cannot sufficiently discrim-

inate between both the models. Therefore, we recommend using the simpler *peak spatial CSF* model.

Conclusions

To establish the relation between the detection of Gabor patterns and discs, we measured the contrast sensitivity for discs of different sizes and colour modulations, which were shown at different luminance levels. Our attempts to explain the data with six models indicate that we most likely detect the edge formed by a disc. The detection thresholds decrease with the length of an edge and the decrease can be explained by a probability summation over multiple edge detectors. A single edge detector can be explained either by the peak sensitivity of the contrast sensitivity function, or using an energy model that integrates of over radially symmetric sinc function.

The current work does not show whether our findings generalise to flickering discs, luminance above 200 cd/m^2 and also to other types of edges. We would like to address these questions in future studies.

Acknowledgements

We would like to thank Scott Daly and anonymous reviewers for all the insightful comments and suggestions. This project has received funding from the European Research Council (ERC) under the European Union's Horizon 2020 research and innovation programme (grant agreement N° 725253–EyeCode).

References

[1] S. Daly, "Visible differences predictor: an algorithm for the assessment of image fidelity," in *Digital Images and Human Vision* (A. B. Watson, ed.), vol. 1666, pp. 179–206, MIT Press, 1993.

[2] P. G. J. Barten, *Contrast sensitivity of the human eye and its effects on image quality*. SPIE Press, 1999.

[3] A. B. Watson and A. J. Ahumada, "The pyramid of visibility," *Human Vision and Electronic Imaging 2016, HVEI 2016*, pp. 37–42, 2016.

[4] R. K. Mantiuk, M. Kim, M. Ashraf, Q. Xu, M. R. Luo, J. Martinovic, and S. Wuerger, "Practical Color Contrast Sensitivity Functions for Luminance Levels up to 10000 cd/m^2," *Color and Imaging Conference*, vol. 2020, pp. 1–6, Nov 2020.

[5] R. K. Mantiuk, M. Ashraf, and A. Chapiro, "Stelacsf: A unified model of contrast sensitivity as the function of spatio-temporal frequency, eccentricity, luminance and area," *ACM Trans. Graph.*, vol. 41, Jul 2022.

[6] O. H. Schade, "Optical and photoelectric analog of the eye," *JOSA*, vol. 46, no. 9, pp. 721–739, 1956.

[7] F. W. Campbell and J. G. Robson, "Application of fourier analysis to the visibility of gratings," *The Journal of physiology*, vol. 197, no. 3, p. 551, 1968.

[8] R. Sekuler, "Spatial vision," *Annual review of psychology*, vol. 25, no. 1, pp. 195–232, 1974.

[9] D. Kelly, "Visual contrast sensitivity," *Optica Acta: International Journal of Optics*, vol. 24, no. 2, pp. 107–129, 1977.

[10] D. H. Kelly, "Motion and vision. ii. stabilized spatio-temporal threshold surface," *JOSA*, vol. 69, no. 10, pp. 1340–1349, 1979.

[11] W. H. Swanson, T. Ueno, V. C. Smith, and J. Pokorny, "Temporal modulation sensitivity and pulse-detection thresholds for chromatic and luminance perturbations," *JOSA A*, vol. 4, no. 10, pp. 1992–2005, 1987.

[12] A. Van Meeteren and J. Vos, "Resolution and contrast sensitivity at low luminances," *Vision research*, vol. 12, no. 5, pp. 825–833, 1972.

[13] J. Mustonen, J. Rovamo, and R. Näsänen, "The effects of grating area and spatial frequency on contrast sensitivity as a function of light level," *Vision research*, vol. 33, no. 15, pp. 2065–2072, 1993.

[14] S. Wuerger, M. Ashraf, M. Kim, J. Martinovic, M. Pérez-Ortiz, and R. K. Mantiuk, "Spatio-chromatic contrast sensitivity under mesopic and photopic light levels," *Journal of Vision*, vol. 20, no. 4, pp. 23–23, 2020.

[15] K. T. Mullen, "The contrast sensitivity of human colour vision to red-green and blue-yellow chromatic gratings.," *The Journal of physiology*, vol. 359, no. 1, pp. 381–400, 1985.

[16] S. M. Wuerger, A. B. Watson, and A. J. Ahumada Jr, "Towards a spatio-chromatic standard observer for detection," in *Human Vision and Electronic Imaging VII*, vol. 4662, pp. 159–172, SPIE, 2002.

[17] E. Howell and R. Hess, "The functional area for summation to threshold for sinusoidal gratings," *Vision research*, vol. 18, no. 4, pp. 369–374, 1978.

[18] J. Rovamo, O. Luntinen, and R. Näsänen, "Modelling the dependence of contrast sensitivity on grating area and spatial frequency," *Vision research*, vol. 33, no. 18, pp. 2773–2788, 1993.

[19] V. Virsu and J. Rovamo, "Visual resolution, contrast sensitivity, and the cortical magnification factor," *Experimental brain research*, vol. 37, no. 3, pp. 475–494, 1979.

[20] M. S. Banks, A. B. Sekuler, and S. J. Anderson, "Peripheral spatial vision: Limits imposed by optics, photoreceptors, and receptor pooling," *JOSA A*, vol. 8, no. 11, pp. 1775–1787, 1991.

[21] C. Carlson, R. Cohen, and I. Gorog, "Visual processing of simple two-dimensional sine-wave luminance gratings," *Vision research*, vol. 17, no. 3, pp. 351–358, 1977.

[22] A. B. Watson and A. J. Ahumada, "A standard model for foveal detection of spatial contrast," *Journal of Vision*, vol. 5, no. 9, pp. 6–6, 2005.

[23] F. W. Campbell, J. J. Kulikowski, and J. Levinson, "The effect of orientation on the visual resolution of gratings," *The Journal of physiology*, vol. 187, no. 2, pp. 427–436, 1966.

[24] D. Regan and K. Beverley, "Visual fields described by contrast sensitivity, by acuity, and by relative sensitivity to different orientations.," *Investigative Ophthalmology & Visual Science*, vol. 24, no. 6, pp. 754–759, 1983.

[25] J. S. Tootle and M. Berkley, "Contrast sensitivity for vertically and obliquely oriented gratings as a function of grating area," *Vision Research*, vol. 23, no. 9, pp. 907–910, 1983.

[26] A. B. Watson and J. I. Yellott, "A unified formula for light-adapted pupil size.," *Journal of Vision*, vol. 12, p. 12, jan 2012.

[27] H. De Lange Dzn, "Research into the dynamic nature of the human fovea→ cortex systems with intermittent and modulated light. i. attenuation characteristics with white and colored light," *JOSA*, vol. 48, no. 11, pp. 777–784, 1958.

[28] G. J. Van Der Horst, "Chromatic flicker," *JOSA*, vol. 59, no. 9, pp. 1213–1217, 1969.

[29] D. Varner, D. Jameson, and L. M. Hurvich, "Temporal sensitivities related to color theory," *JOSA A*, vol. 1, no. 5, pp. 474–481, 1984.

[30] M. R. B. Pérez, "Measuring the temporal contrast sensitivity function for isoluminant chromatic flicker stimuli," Master's thesis, Eindhoven University of Technology, 2017.

[31] X. Kong, M. R. Bueno Pérez, I. M. Vogels, D. Sekulovski, and I. Heynderickx, "Modelling contrast sensitivity for chromatic temporal modulations," in *Color and Imaging Conference*, vol. 2018,

pp. 324–329, Society for Imaging Science and Technology, 2018.

[32] S. Hecht and S. Shlaer, "Intermittent stimulation by light: V. the relation between intensity and critical frequency for different parts of the spectrum," *The Journal of general physiology*, vol. 19, no. 6, pp. 965–977, 1936.

[33] E. Hartmann, B. Lachenmayr, and H. Brettel, "The peripheral critical flicker frequency," *Vision Research*, vol. 19, no. 9, pp. 1019–1023, 1979.

[34] A. Raninen and J. Rovamo, "Perimetry of critical flicker frequency in human rod and cone vision," *Vision research*, vol. 26, no. 8, pp. 1249–1255, 1986.

[35] K. K. De Valois, R. L. De Valois, and E. W. Yund, "Responses of striate cortex cells to grating and checkerboard patterns.," *The Journal of Physiology*, vol. 291, no. 1, pp. 483–505, 1979.

[36] CIE170-1:2006, "Fundamental chromacity diagram with psychological axes - part 1," tech. rep., Central Bureau of the Commission Internationale de l' Éclairage, 2016.

[37] A. M. Derrington, J. Krauskopf, and P. Lennie, "Chromatic mechanisms in lateral geniculate nucleus of macaque.," *The Journal of physiology*, vol. 357, no. 1, pp. 241–265, 1984.

[38] A. B. Watson and D. G. Pelli, "Quest: A bayesian adaptive psychometric method," *Perception & psychophysics*, vol. 33, no. 2, pp. 113–120, 1983.

[39] M. Kleiner, D. Brainard, and D. Pelli, "What's new in psychtoolbox-3?," 2007.

[40] J. Foley, S. Varadharajan, and C. Koh, "Detection of Gabor patterns of different sizes, shapes, phases and eccentricities," *Vision research*, 2007.

[41] D. M. Levi and R. S. Harwerth, "Psychophysical mechanisms in humans with amblyopia.," *American journal of optometry and physiological optics*, vol. 59, no. 12, pp. 936–951, 1982.

[42] J. Verbaken and A. Johnston, "Population norms for edge contrast sensitivity.," *American Journal of Optometry and Physiological Optics*, vol. 63, no. 9, pp. 724–732, 1986.